Journal of Drug Delivery Science and Technology 82 (2023) 104362

Contents lists available at ScienceDirect

Journal of Drug Delivery Science and Technology

journal homepage: www.elsevier.com/locate/jddst

Sorafenib loaded ZIF-8 metal-organic frameworks as a multifunctional nano-carrier offers effective hepatocellular carcinoma therapy

Derya Mete [a], Egehan Yemeztaşlıca [a], Gülşah Şanlı-Mohamed [a,b,*]

[a] Department of Chemistry, İzmir Institute of Technology, 35430, İzmir, Turkey
[b] Department of Biotechnology and Bioengineering, İzmir Institute of Technology, 35430, İzmir, Turkey

ARTICLE INFO

Keywords:
Hepatocellular carcinoma
Sorafenib
Metal-organic frameworks
ZIF-8
Controlled drug release

ABSTRACT

Hepatocellular carcinoma (HCC) is a primary malignant neoplasia of the liver and sorafenib is one of the most commonly used drugs in the treatment of HCC. Due to undesirable nature and side effects of sorafenib, nano-drug delivery systems are being developed. A member of metal-organic frameworks (MOFs), ZIF-8 offers a very suitable platform for drug transport and controlled drug release due to its zinc content and pH-sensitive, biodegradable in an acidic environment. In the present study, sorafenib was encapsulated in ZIF-8 material with 53.8% efficiency and 58% loading capacity (SRF@ZIF-8). Structural characterizations of synthesized ZIF-8 and SRF@ZIF-8 system were investigated in details. Drug release analysis exhibited a faster release profile at pH 5.0 compared to that of pH 7.4. The cytotoxic effects of sorafenib and zinc were investigated in HepG2 and HuH-7 cell lines in vitro. The results demonstrated that in addition to sorafenib, ZIF-8 provided zinc to the environment with its biodegradable structure resulted in an effective cytotoxic effect on HCC cells. The findings showed that a formulation combining zinc and sorafenib together was more effective in HCC treatment compared to sorafenib itself.

1. Introduction

Hepatocellular carcinoma (HCC) is primary malignant neoplasia of the liver, which is more common in populations with a high incidence of hepatitis. According to world statistics, HCC is the fifth most common type of cancer and the third leading cause of cancer-related deaths [1,2]. Approximately 250,000–1,000,000 people die as a result of HCC every year. While most types of cancer can be treated with applications such as surgical intervention, radiotherapy, and chemotherapy [3] depending on their localization and stages, most patients are diagnosed at a late stage of HCC because of the absence of the early and pathognomonic symptoms of HCC. As a result, most of the cases are cirrhotic at the time of diagnosis and are in a stage that cannot be effectively treated [4,5]. This situation makes it necessary to seek new effective alternative ways of treatment for HCC.

Sorafenib (SRF), a multiple kinase inhibitor, is one of the most commonly used drugs in the treatment of HCC [5,6]. It is the first Food and Administration (FDA) approved drug for systemic therapy in HCC patients, and studies show that sorafenib has a life-extending effect in advanced HCC. The hydrophobic structure, low solubility and stability of Sorafenib, decreasing its effectiveness without going to the liver, having undesirable side effects, and damaging healthy tissues other than cancerous tissue limit the applications of this molecule in treatment [7,8]. Today, nano-drug delivery systems are being developed to eliminate these and similar problems that can be seen also in other chemotherapy drugs [9]. There is an increasing interest in the development of active substance-loaded nano-carrier systems for therapeutic purposes [10]. These systems provide controlled release, biocompatibility, solubility, targeting, stability, non-toxic and non-carcinogenic property in biological systems. Several kinds of research also have been performed towards the development of new generation drug platforms and drug delivery systems to make HCC cells susceptible to sorafenib.

There is distinct importance of zinc in HCC. Compelling evidence supports the plausibility that a zinc treatment regimen will prevent the development of malignancy and termination of progressing malignancy in HCC [11,12]. This has led to the development of zinc-based treatments for HCC and the search for an agent to provide zinc to the cell. Therefore there is a need to develop new formulations for HCC treatment as anticancer metallodrugs, including zinc.

In recent years, metal-organic frameworks (MOFs), which have attracted the attention of chemistry and materials science researchers, are emerging as a new material to be used in nanomedical applications.

* Corresponding author. Izmir Institute of Technology, Science Faculty, Department of Chemistry Urla, Izmir, Turkey.
E-mail addresses: gulsahsanli@iyte.edu.tr, gulsahsanli@hotmail.com (G. Şanlı-Mohamed).

https://doi.org/10.1016/j.jddst.2023.104362
Received 24 December 2022; Received in revised form 8 March 2023; Accepted 11 March 2023
Available online 15 March 2023

MOFs are crystalline, porous, and high-volume materials that are formed by the self-polymerization of metal-ion and organic multi-toothed ligands. Due to their outstanding properties like well-defined pore opening, regular structure, adjustable size, versatile functionality, high loading capacity, and biocompatibility, many potential application areas of MOFs have been explored lately such as catalyst, magnetic devices, ion exchange, gas storage, separation, and drug transport [13]. ZIF-8, created with zinc metal ion and 2-methylimidazole, is an important member of the MOF family. ZIF-8, which has all the superior properties of MOFs, is a very suitable platform for drug delivery and controlled drug release due to its zinc content and its biodegradability in an acidic environment as pH-sensivite. So far, various molecules such as methyl orange, methylene blue, caffeine, cyt-c enzyme, turmeric, 3-methilladenine (3-MA), insulin were successfully encapsulated in the cavities of ZIF-8 for several purposes. Additionally, ZIF-8 was utilized as drug delivery systems for doxorobusin, 5-Fluorouacil, camptothecin, 6-mercaptopurine. The only study regarding to HCC has been shown in gabapentin-ZIF-8 against HepG2 liver cancer cells but no study was conducted in which sorafenib encapsulated with ZIF-8 [14].

In this research, it was aimed to improve HCC treatment by encapsulation of sorafenib drug with ZIF-8 metal-organic frameworks as a multifunctional nano-carrier. The purpose of this encapsulation was to increase the accumulation of sorafenib in liver tissue by taking advantage of the pH sensitivity of ZIF-8, and at the same time to minimize the damage of the drug to healthy tissues. In addition, since ZIF-8 biodegradable structure provides zinc which creates a cytotoxic effect on HCC cells, the cytotoxic effects of sorafenib and zinc were combined as dual therapy in a single nanoparticle. Herein, sorafenib drug was encapsulated in ZIF-8 material (SRF@ZIF-8) with 53.8% yield and 58% loading capacity. Drug release analysis performed after detailed structural characterization of synthesized ZIF-8 and SRF@ZIF-8 system was observed to exhibit a slower profile at pH 7.4, while fast at pH 5. The cytotoxic effects of sorafenib, ZIF-8 and SRF@ZIF-8 were investigated in HepG2 and HuH-7 cell lines in vitro. SRF@ZIF-8 demonstrated a better cytotoxic effect on HCC cells compared to sorafenib and ZIF-8 because the biodegradable structure of ZIF-8 has provided not only sorafenib but also zinc to the environment. It has been also observed that the synthesized multifunctional nano-carrier enters the nucleus in HCC cells and exerts an apoptotic effect. As a result of this study, the findings obtained showed that a formulation with ZIF-8 metal-organic frameworks as a multifunctional nano-carrier combining zinc and sorafenib together was more effective on HCC treatment.

2. Materials and methods

2.1. Materials

Unless otherwise stated all chemicals were purchased from Sigma.

2.2. Synthesis of ZIF-8 and SRF@ZIF-8nanoparticles

The synthesis of ZIF-8 nanoparticles was carried out with the some modifications of the previously establised method of Pan et al. (2011) [15]. In this study, ZIF-8 was synthesized such that the Zn^{+2}:2-methylimidazole:H_2O molar ratio of 1:70:1238 was obtained [16]. According to these values, $Zn(NO_3)_2.6H_2O$ (585 mg) was completely dissolved with 4 mL of DI water. On the other side, 2-methylimidazole (2-MeIM) (11.35 g) was dissolved in 40 mL of DI water and 6 mL of DMSO solution was added. Then two solutions were mixed together to form a white solution and the mixing process was continued for another 5 min at room temperature. The samples as white powders were collected by centrifugation at 14,000 rpm for 15 min, washed three times with 30% ethanol and then dried.

For the synthesis of SRF@ZIF-8 nanoparticles, the same method described above was applied. In this study, 50 mg of Sorafenib was dissolved in 6 mL of DMSO and added to the dissolved 2-methylimidazole solution and then added to the dissolved zinc nitrate solution after stirring for 5 min. Other steps were continued as the ZIF-8 synthesis.

2.3. Nanoparticle yield and encapsulation efficiency

The yield of the nanoparticles was determined by gravimetry after washing and drying of a known volume of nanoparticle suspension. The drug encapsulation efficiency was investigated directly by inductively coupled plasma-optical emission spectrometry (ICP-OES). In ICP-OES analysis the particles were decomposed in an aqueous solution of 5% HNO_3 prior to the measurement, and thus, the Zn compositions of the whole particle material were obtained. The encapsulation efficiency of the active agent was calculated as follows:

Encapsulation efficiency (%) = (mass of drug in nanocrystals/mass of total loaded drug) × 100 100

2.4. Characterization of ZIF-8 and SRF@ZIF-8 nanoparticles

Particle sizes and zeta potentials of ZIF-8 and SRF@ZIF-8 nanoparticles were determined by Dynamic Light Scattering Method (DLS) via Zetasizer Nano Z Malvern Panalytical, United Kingdom). The dimensions of the nanoparticles were verified by scanning electron microscopy (SEM). The samples were displayed using the 5 KV electron beam and 200 nm scale by the FEI QUANTA 250 FEG (USA). The average fibre diameter was evaluated from the SEM micrographs of 100 individual fibres by using Fiji ImageJ software. Energy Dispersive X-ray Spectroscopy (EDX) were used to determine the elemental compositions of ZIF-8 and SRF@ZIF-8 nanoparticles. XRD analysis was performed by using the CuKα radiation in the Philips X'arakpert Pro (Royal Philips Electronics, Amsterdam, The Netherlands) diffractometer with a beam length of 1.541 A, at 40 kV and 25 mA. With the Fourier Transform Infrared Analysis (FT-IR) (PerkinElmer FT-IR System Spectrum BX), the functional groups present in ZIF-8 and SRF@ZIF-8 were examined.

2.5. Determination of Zn^{2+} concentration

ZIF-8 and SRF@ZIF-8 nanoparticles were dissolved in three different pH environments in phosphate-citrate buffer at pH 5 and 6 and PBS at pH 7.4. Samples agitated at 150 rpm were centrifuged after 5 days and the supernatants were analyzed by Flame Atomic Absorption Spectroscopy at a wavelength of 213.9 nm.

2.6. Hemolysis

To determine hemolysis potential of nanoparticles, erythrocytes were mixed with nanoparticles at 1, 5 and 10 μg/mL ZIF-8 and SRF@ZIF-8 (in PBS solution) at 1:1 (v/v) ratio and incubated at 37 °C for 4 h. PBS was used as negative control group and 1% Triton X-100 as positive control group. At the end of the incubation, erythrocytes and nanocrystals were separated from mixture by centrifugation and hemoglobin was spectrophotometrically determined at upper layer at 540 nm. Hemolysis ratio calculated via absorbance with the formula below.

(% Hemolysis = (A sample - A negative control)*100/A positive control)

2.7. Release of sorafenib from Sorafenib@ZIF-8

A typical release system was used by suspending 25 mg of ZIF-8 and SRF@ZIF-8 nanoparticles in 20 mL of PBS solution (pH 7.4 and 5.0 and) at 37 °C and maintained under shaking (shaking frequency = 150 rpm). At each time 1 mL of sample were taken and centrifuged to collect the

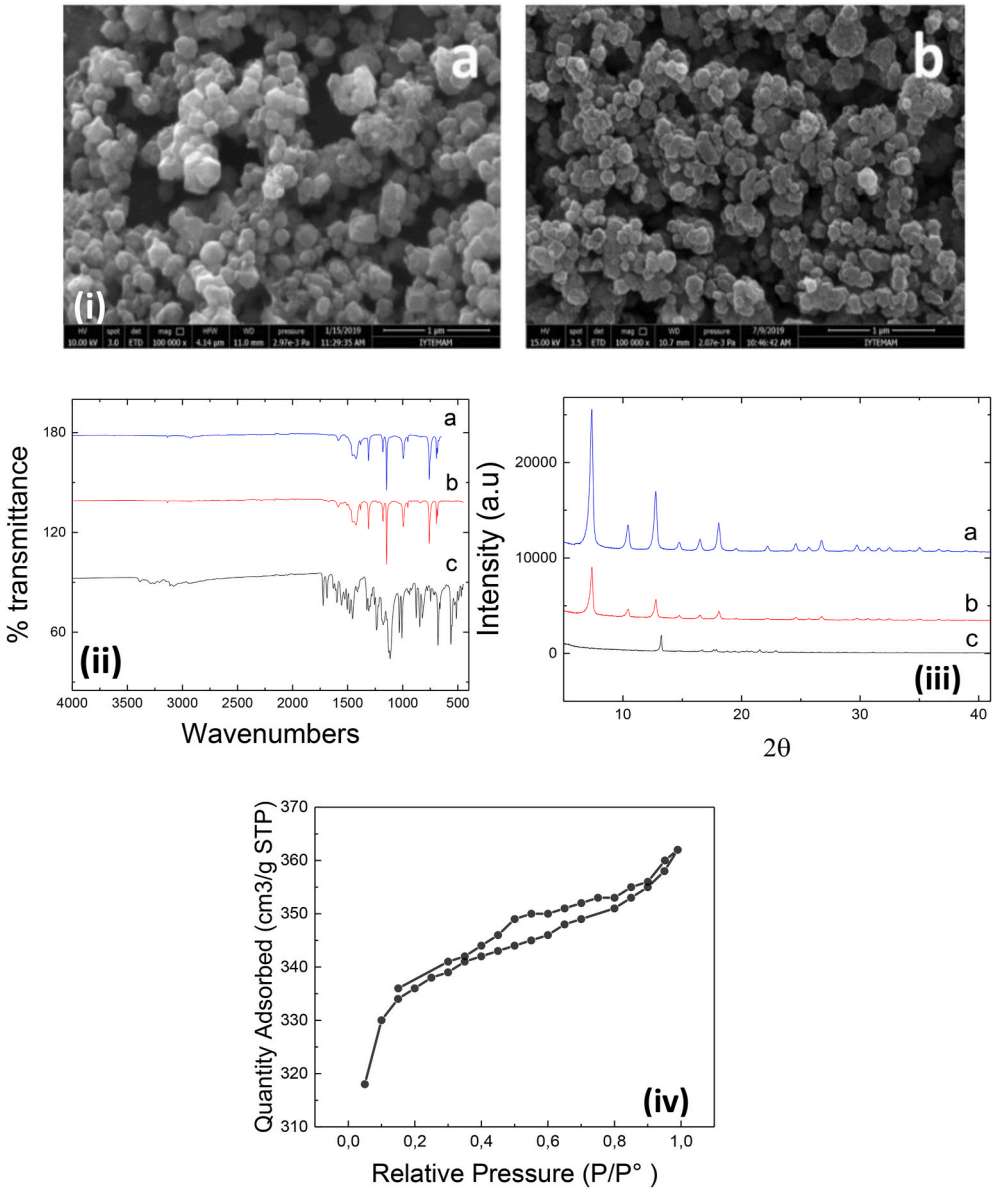

Fig. 1. (i) SEM micrographs of a)ZIF-8 b)SRF@ZIF-8; (ii) FTIR spectra for a) ZIF-8 b) SRF@ZIF-8 and c) SRF; (iii) XRD patterns of a)ZIF-8, b)SRF@ZIF-8 and c)SRF; (iv) N2 adsorption/desorption slope of ZIF-8.

Table 1
Yield, Hydrodynamic radius, Drug Loading Capacity, and Zeta Potentials of a) ZIF-8 and b) SRF@ZIF-8.

	Yield (%)	Hydrodynamic radius (nm)	Drug Loading Capacity (%)	Zeta Potential (mV)
ZIF-8	**68,3**	**340**		**−21,3**
SRF@ZIF-8	**53,8**	**809**	**58**	**17,8**

supernatant and at the same time system was replaced with fresh PBS. The UV–Visible spectroscopy absorbance value of each sample was recorded at 265 nm.

The release percentage of Sorafenib was determined according to the following formula:

Release percentage (%) = Mr/Mt, where Mr is the amount of released Sorafenib, while Mt is the total amount of loaded Sorafenib

2.8. Cell viability and cytotoxicity test

HuH-7 and HepG2 cell lines were cultured in DMEM medium containing 1% penicillin/streptomycin, 1% L-glutamine and 10% fetal bovine serum. The cells at a concentration of 5000 cells/well were seeded into 96-well cell culture dishes and incubated for 24 h at 37 °C, 95% humidity and 5% CO_2. Then the cells were incubated with ZIF-8 and SRF@ZIF-8(sterilized by UV irritation) at various concentrations for 24, 48 and 72 h. At the end of each incubation period, 10 μl of MTT solution was added and incubated at 37 °C for 4 h, then formazan crystals were dissolved with DMSO (dimethyl sulfoxide) and measured at 570 nm.

2.9. Apoptosis analysis

To understand the effect of Sorafenib, ZIF-8 and SRF@ZIF-8nanoparticles on hepatocellular carcinoma cells, Annexin V-FITC detection kit was used. For this analysis, 1980 μL of cell suspension with density 5×10^5 cells were seeded in 6-well plates and incubated for 24 h

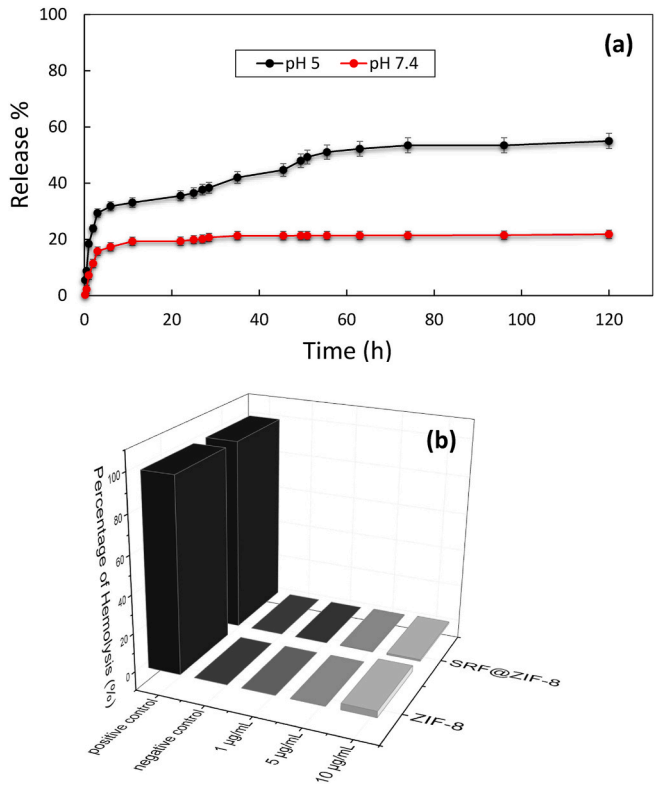

Fig. 2. (a) Drug release profile of SRF from ZIF-8 (b) Hemolysis rates of ZIF-8 and SRF@ZIF-8 nanoparticles.

at 37 °C, 95% humidity and 5% CO_2. After incubation, Sorafenib, ZIF-8 and SRF@ZIF-8nanoparticles were dissolved in DMSO and added to incubated cells at final volume of 2 mL of various concentrations, respectively. The treated cells were incubated for 24 and 48 h in CO_2 incubator at 37 °C. At the end of each incubation period, the cells were harvested by trypsin and centrifuged at 800 rpm for 5 min. The resulting pellets were dissolved in 5 mL of PBS and centrifuged again. After centrifugation, the pellet was dissolved in 250 µL binding buffer and 2 µL Annexin V-FITC and 5 µL propidium iodide were added. The stained cells were incubated for 15 min at room temperature and the apoptotic effects of test compounds were determined by flow cytometer.

2.10. Cell cycle analysis

The effects of ZIF-8 and SRF@ZIF-8 nanoparticles on the cell cycle were tested in HuH-7 and HepG2 cancer cell lines by propidium iodide staining (BioVision, USA). Into 6-well plates, 1980 µL of cell suspension at a density of 5×10^5 cells per well were inoculated and incubated for 24 h. Test compounds were dissolved in DMSO and added to cells to maintain the final concentrations of 5, 10, 20, 50, 100 µg/mL. The cells treated with test compounds were incubated for 24 h in a CO_2 incubator at 37 °C.

After incubation, cells were harvested by trypsin and centrifuged at 1200 rpm for 10 min. The supernatant was poured, and the pellet was dissolved in 5 mL of PBS. The cell suspension was centrifuged again. The pellet was resuspended in 1 mL cold PBS and fixed by adding 4 mL of −20 °C ethanol (99.8%) on a low-speed vortex. The fixed cells were incubated at −20 °C for at least 24 h. After incubation, the fixed cell suspension was centrifuged at 1200 rpm for 10 min at 4 °C. The pellet was dissolved in 5 mL of PBS and centrifuged again. The pellet was resuspended in a 200 µL phosphate buffer, including 0.1% Triton X-100. 20 µL RNase A (200 µg/mL) was added to the cell suspension, and cells were incubated in a CO_2 incubator at 37 °C for 30 min. After incubation, 20 µL PI (1 mg/mL) was added, and cells were incubated at room temperature for 15 min. The cell cycle distribution was determined by flow cytometer (BD FACSCanto, USA), and data were analyzed by ModFit LT software. For each sample, at least 10,000 events were collected.

2.11. Data presentation and statistical analysis

All experiments were performed at least in duplicate. Statistical errors of the data were determined by GraphPad Prism version 8.00 for Windows (GraphPad Software, La Jolla, CA, USA) (www.graphpad.com).

3. Results and discussion

3.1. Synthesis and characterization of ZIF-8 and SRF@ZIF-8nanoparticles

ZIF-8 nanoparticles were synthesized successfully in a Zn^{+2}:2-methylimidazole: H_2O molar ratio of 1: 70: 1238 and sorafenib was encapsulated into ZIF-8 in situ. Scanning electron microscopy (SEM) showed that the ZIF-8 and SRF@ZIF-8 materials consisted of isolated crack-free particles of diameter between 113 and 140 nm. As shown in Fig. 1(i), scanning electron microscopy (SEM) images of the resulting structures indicate the formation of rhombic dodecahedral crystals, which corresponds to the average size of biomedically relevant ZIF-8 encapsulating biomacromolecules, as previously reported by Falcaro and co-workers [17]. As expected,energy-dispersive X-ray (EDX) spectroscopy maps confirm the presence of Zn, C, and N elements uniformly distributed throughout each crystal whereas, sorafenibe has F,S and Cl [18]. The atomic percent distribution of ZIF-8 is in accordance with the $C_8H_{10}N_4Zn$ formula. When the distribution of SRF@ZIF-8 and ZIF-8 nanoparticles is compared, it is observed that the F and Cl elements from SRF are added in the atomic percentage distribution of SRF@ZIF8 and the percentage of element C increases. These results overlap with the SRF with the formula $C_{21}H_{16}ClF_3N_4O_3$.

Comparison of the sample XRD results to the pattern simulated from the published ZIF-8 structure data indicates that the product is pure-phase ZIF-8 material. Peak broadening can be clearly observed from the sample XRD pattern, indicating the formation of nanosized crystals [19]. Each synthesis yielded pure-phase ZIF-8 crystals as demonstrated by X-ray diffraction (XRD) patterns (Fig. 1(iii)). Patterns generated by the ordered porous structure of the ZIF-8 particles between 2θ values of 5 and 40° can be observed and the peak broadening observed indicates the formation of nanosized crystals. The relative intensities and the sharp peaks in the diffraction pattern of ZIF-8 at $2\theta = 7.11°$, 12.5°, 17.75°, and 26.4° prominent peak positions, including 011, 002, 112, 022, 013, and 222 are in good agreement with previous reports [20,21], confirming the sodalite structure, which is the typical structure of ZIF-8, and the well-defined peaks revealed high crystallinity. The interplanar spacings calculated using Bragg's law from the reflection at different Bragg's angles correspond to a body centered cubic structure with a unit cell parameter of 17 Å and are in accordance with those reported in the literature [20,21]. The XRD analysis show the exact crystal structure of ZIF-8 nanoparticles showing that the addition of SRF didn't alter the lattice parameters of ZIF-8.

The zeta potential of nanoparticles is an important factor for cellular retention rate in in vitro applications. Therefore, zeta potential and hydrodynamic radii of ZIF-8 and SRF@ZIF-8 nanoparticles were investigated by DLS measurement (Table 1). The hydrodynamic radius of the ZIF-8 nanoparticles were approximately two times larger than the values in the SEM measurement [22]. Also, the zeta potentials of the nanoparticles were measured as 24.5 and 17.8 mV, respectively. This change in zeta potential can be attributed to the encapsulation of the drug.

FTIR spectra were obtained for ZIF-8, Sorafenib, and SRF@ZIF-8 (Fig. 1(ii)). In the spectrum corresponding to ZIF-8, two bands at 3135 and 2928 cm^{-1} can be observed for the aromatic C–H stretch and the

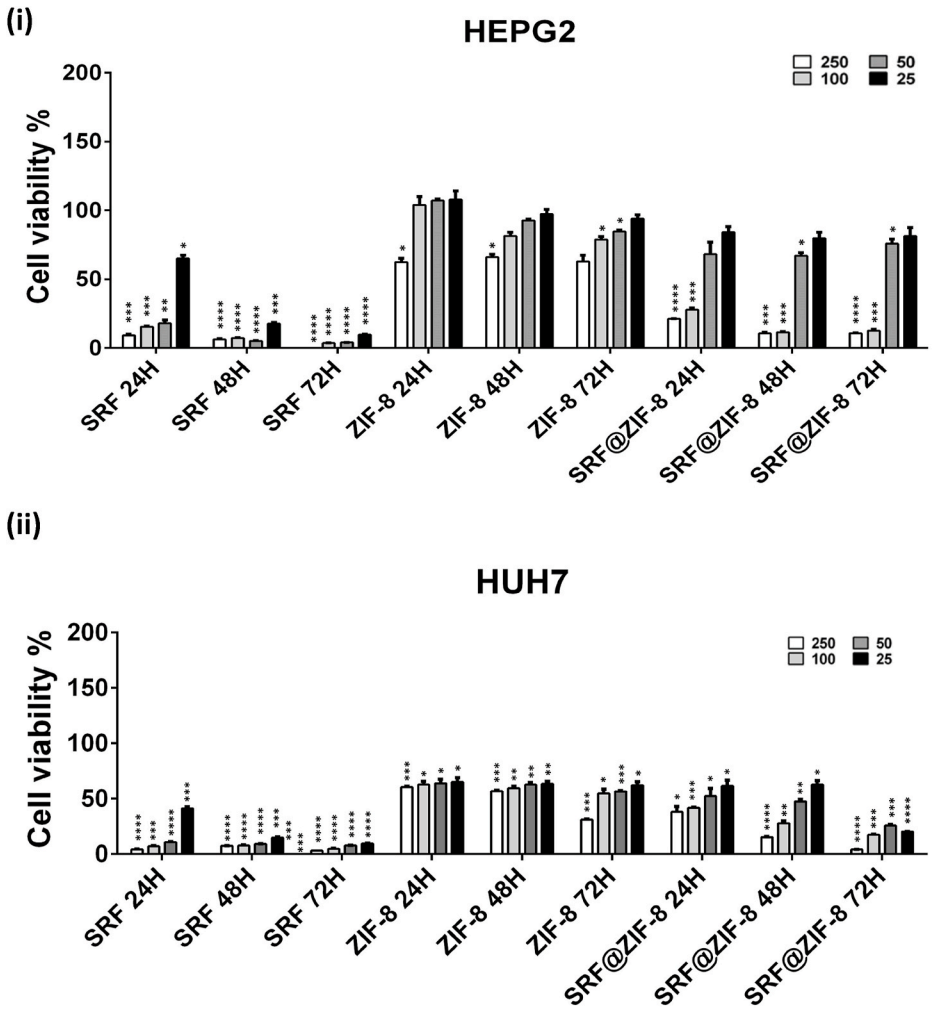

Fig. 3. Cytotoxic activity profiles of SRF, ZIF-8, and SRF@ZIF-8 in (i) HEPG2 and (ii) HUH7 cell lines at 24, 48, and 72 h. Statistical analysis was performed with one-way ANOVA and p values are <0.0001 in ****, <0.001 in ***, <0.01 in ** and <0.05 in * indicating that results are statistically significant.

aliphatic C–H stretch of the imidazole, respectively. The 1606 cm^{-1} band is for the C–C stretch, and the peak at 1580 cm^{-1} is for the C–N stretch. The C–N absorption bands are found in the 1100–1400 cm^{-1} region. The absorption band at 421 cm^{-1} is associated with the Zn–N stretching mode. These assignments are in agreement with the FTIR measurements from Park et al. [23]. Several bands are observed for SRF@ZIF-8. The FTIR spectrum analysis for the system SRF@ZIF-8 do not undoubtedly show the adsorption of the drug into ZIF-8, but the detection of characteristic bands for both ZIF-8 and drug indicates the presence of both compounds.

Metal organic frameworks are organic coordination compounds with high porosity. The surface areas of these materials are quite large. Therefore, the N_2 adsorption/desorption slopes of the ZIF-8 nanoparticles were deduced (Fig. 1 (iv)). The curve obtained corresponds to the Type I isotherm. Thanks to this measurement, it is calculated that the nanoparticles have 1017.3249 m^2/g and 1495.7186 m^2/g BET and Langmuir surface areas. The surface area results found correspond to those known in the literature [24].

Our first aim in this study is to synthesize nanoparticles that can be encapsulated in small size with high loading and high encapsulation efficiency of sorafenib. ICP-OES was used to determine the effective SRF loading capacity. In the ICP-OES analysis, nanoparticles were degraded in 5% HNO_3 solution before measurement and thus the amount of Zn in the nanoparticle was obtained. Based on the Zn amount obtained, the ZIF-8 yield was calculated. The amount of SRF in ZIF-8 using the gravimetrically determined ZIF-8 and SRF@ZIF-8 quantities is shown in Table 1.

In order to observe the change of drug release from SRF@ZIF-8 nanoparticles over time, pH 5 solution mimicking acidic cancer cell environment and PBS buffer solutions with physiological pH 7.4 were created. SRF@ZIF-8 nanoparticles were incubated in these two different pH environments at 150 rpm for 5 days. Absorbance values of supernatants were measured with UV–Vis device to calculate the amount of drug released in a certain time period. The cumulative emission graph obtained at pH 5 and 7.4 is in Fig. 2(a).

Erythrocytes, also known as red blood cells, constitute 48% of blood. The erythrocytes-MOFs interaction is essential to study the hemoglobin release known as hemolysis. The percentage of erythrocyte cells in the blood of ZIF-8 and SRF@ZIF-8 nanoparticles were investigated. It is known that increased concentration of nanoparticles and especially positive surface charged nanoparticles undergo more hemolysis by erythrocytes in blood than negatively charged ones [25]. The hemolysis rate of nanoparticles on erythrocytes was investigated in three different concentrations: 1 μg/mL, 5 μg/mL, and 10 μg/mL. The hemolysis rate of nanoparticles was found to be consistent with each other as 0.53% and 0.42%, respectively (Fig. 2(b)). These values are below 5%, which supports the biocompatibility of nanoparticles.

Cell viability of ZIF-8 and SRF@ZIF-8 nanoparticle concentrations (25–250 μg/mL) at 24, 48 and 72 h in HEPG2 and HuH-7 cell lines was examined using the MTT assay (Fig. 3). It is known by the literature that

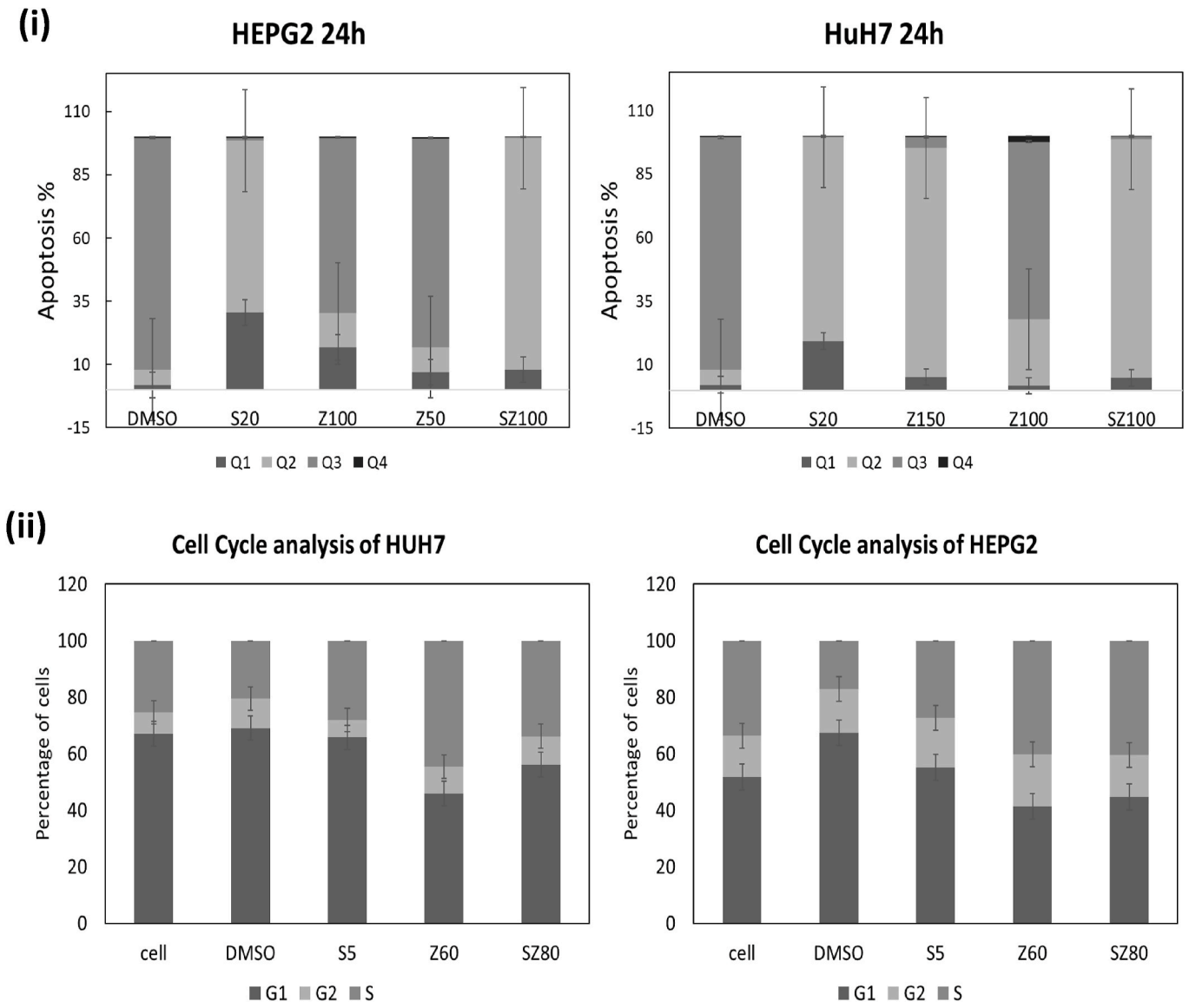

Fig. 4. (i) Apoptosis analysis of SRF, ZIF-8 and SRF@ZIF-8 at 24 h in HEPG2 and HUH7 cell lines (necrosis (Q1), late apoptosis (Q2), viability (Q3) and early apoptosis (Q4) rates); (ii) The cell cycle analysis for of SRF, ZIF-8 and SRF@ZIF-8 at 24 h in HEPG2 and HUH7 cell lines.

an amount less than 30 μg/mL ZIF-8 does not have a cytotoxic effect on cells. When the results obtained are examined, nearly 100% of the cells preserved their viability at 25 μg/mL ZIF-8 and these results are consistent with the literatüre [26]. While 250 μg/mL ZIF-8 showed approximately 60% viability on both cell lines, it was observed that it was not cytotoxic at lower concentrations. The incubation time of ZIF-8 is not an important factor for the decrease in cell viability. As a result of the MTT test, it is shown that SRF@ZIF-8 nanoparticles create a significant cytotoxic effect on HEPG2 and HuH-7 cells compared to ZIF-8. Cell death by the addition of Sorafenib to ZIF-8 was found to be more effective in the HEPG2 cell line than HuH-7 cells (Fig. 3). The results were Statisticaly analyzed with one-way ANOVA and p values are <0.0001 in ****, <0.001 in ***, <0.01 in ** and <0.05 in * indicating that results were statistically significant. While SRF@ZIF-8 nanoparticles in HEPG2 cells decreased by 40% at a dose of 250 μg/mL and at the end of 24 h, in HuH-7 cells this ratio decreased by 20%. In both cell lines, cell viability showed an inversely proportional effect due to the increasing dose of SRF@ZIF-8 nanoparticles. Along with the increase in incubation time, it was observed that SRF@ZIF-8 nanoparticles also increased cellular inhibition (Fig. 3). High cytotoxic effects were observed with Sorafenib in HuH-7and HEPG2 cell lines. The low cytotoxicity of SRF@ZIF-8 compared to SRF on cell death can be explained by the slow release of the drug.

Nanoparticles can diffuse passively into the cytoplasm and other cell organelles through endocytosis. This may cause the formation of nanoparticle agglomerates inside the cell. The interaction between metal-containing nanoparticle aggregates and living cells leads to cell death. This is observed more clearly with morphological changes, incubation time and increase in nanoparticle concentration. The HepG2 cell line was examined in a 24-h period, when the values of 20 μg/mL Sorafenib and 100 μg/mL SRF@ZIF-8 were compared, it was observed that the apoptosis rate increased from 68.0% to 91.5%, while the rate of necrosis decreased from 30.5% to 8.0%. The HuH-7 cell line was examined in a 24-h period, when the 50 μg/mL Sorafenib and 100 μg/mL SRF@ZIF-8 values were compared, it was observed that the apoptosis rate increased from 80.1% to 93.9%, while the necrosis rate decreased from 19.3% to 4.8% (Fig. 4(i)). The rate of apoptosis was increased and the desired reduction in the rate of necrosis was achieved. In addition, when the viability rates in the cell are examined, it has been shown that the decrease in the survival rate in the SRF@ZIF-8 is compatible with the results of apoptosis. In addition, when evaluated in terms of the effects of ZIF-8 concentration on cell viability, apoptosis results were observed to

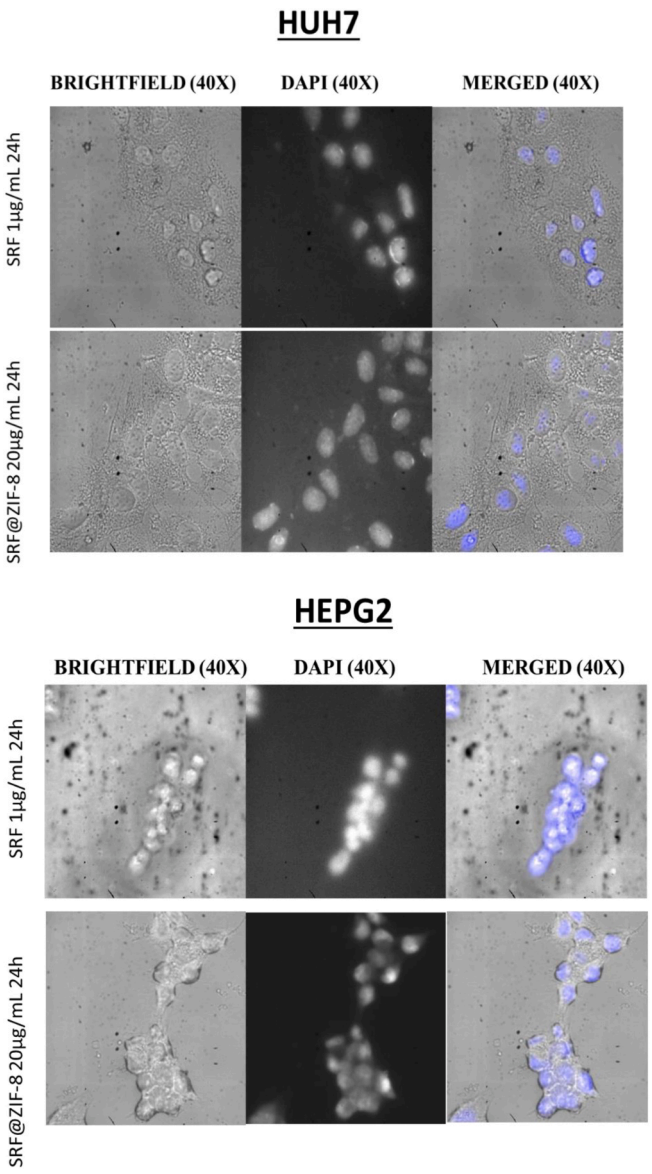

Fig. 5. Confocal images of SRF and SRF@ZIF-8 at 24 hours in HUH7 and HEPG2 cell lines.

be consistent with MTT results. According to the literature, Sorafenib is known to downregulate Cyclin D1 and Cyclin D3 & CDK4 proteins [27]. It is also known that the aforementioned proteins are involved in passing the G1 phase, one of the cell cycle control phases. When the results are examined comparatively, the findings showing that the highest amount of HepG2 and HuH-7 cells was found in the G1 phase (Fig. 4(ii)) is consistent with the literature [28].

The confocal microscope image results of Sorafenib and SRF@ZIF-8 were examined, accumulation around this region including the cell nucleus was observed by DAPI staining (Fig. 5). The organelles of the nucleus, nucleus membrane and endoplasmic reticulum (ER) are closest to these regions. Sorafenib is known to cause stress on the ER [29]. Nucleus, nuclear membrane and endoplasmic reticulum; It forms the endomembrane complex with the Golgi device and functions together. The accumulation of sorafenib in the specified regions is known to be associated with the kinase inhibition activity stated as previously [28, 29]. Sorafenib, known as a multikinase inhibitor, is thought to cause stress by affecting the organelles that cooperate with ER and disrupting their work since its activity takes place in these regions.

4. Conclusions

In this study, a new generation smart, biocompatible, biodegradable and multifunctional nano-carrier system has been developed, well-characterized and its cytotoxic effect has been investigated for the treatment of HCC. In this direction, sorafenib used in HCC treatment was encapsulated in ZIF-8 smart material formed with zinc and 2-methylimidazole by the one-pot method with 53.8% efficiency and 58% loading capacity. The material obtained has been characterized structurally and functionally in detail. SEM images showed that SRF@ZIF-8 nanoparticles were homogeneously distributed and the structure was rhombic dodecahedral with nearly 100 nm in size. The zeta potential results demonstrated that SRF@ZIF-8 nanoparticles were negatively charged and thus suitable for targeting. The crystallinity and impurity of nanoparticles were determined by XRD measurement. The drug release profile was indicated that sorafenib released faster at acidic pH which belongs to the tumor microenvironment compared to physiological pH. The synthesized SRF@ZIF-8 nanoparticles were also demonstrated as biocompatible and biodegradable. Besides, as a delivery system, ZIF-8 was chosen for its therapeutic and treatment-supporting effect because of the zinc source in this study. It was aimed to create a dual cytotoxic effect on HCC by combining the effects of zinc and sorafenib on a single platform. The results demonstrated that SRF@ZIF-8 nanoparticles provided better cytotoxicity on HepG2 and HuH-7 cell lines compared to sorafenib and zinc itself. As a result of this study, the findings showed that Sorafenib loaded ZIF-8 metal-organic frameworks as a multifunctional nano-carrier provided effective therapy for hepatocellular carcinoma.

Ethical approval

Not applicable.

Consent to participate

Not applicable.

Consent to publish

Not applicable.

Authors contributions

DM: Methodology, Investigation, Data curation, Formal analysis, original draft preparation. EY: Methodology, Data curation, Formal analysis GSM: Supervision, Conceptualization, Investigation, Writing - review & editing.

Funding

The study was supported by The Scientific & Technological Research Council of Turkey (TUBITAK, Project number, KBAG–119Z023).

Availability of data and materials

The data that support the findings of this study are available from the corresponding author, upon reasonable request.

Declaration of competing interest

The authors declare that they have no known competing financial interests or personal relationships that could have appeared to influence the work reported in this paper.

Data availability

Data will be made available on request.

Acknowledgments

The authors would like to thank Biotechnology and Bioengineering Application and Research Center (BIOMER) and The Center for Materials Research (IZTECH-CMR) at İzmir Institute of Technology for the facilities and technical support.

References

[1] J. Ferlay, H.-R. Shin, F. Bray, D. Forman, C. Mathers, D.M. Parkin, Estimates of worldwide burden of cancer in 2008: GLOBOCAN 2008, Int. J. Cancer 127 (2010) 2893–2917, https://doi.org/10.1002/ijc.25516.

[2] A. Jemal, F. Bray, M.M. Center, J. Ferlay, E. Ward, D. Forman, Global cancer statistics, CA A Cancer J. Clin. 61 (2011) 69–90, https://doi.org/10.3322/caac.20107.

[3] D. Dimitroulis, C. Damaskos, S. Valsami, S. Davakis, N. Garmpis, E. Spartalis, A. Athanasiou, D. Moris, S. Sakellariou, S. Kykalos, G. Tsourouflis, A. Garmpi, I. Delladetsima, K. Kontzoglou, G. Kouraklis, From diagnosis to treatment of hepatocellular carcinoma: an epidemic problem for both developed and developing world, World J. Gastroenterol. 23 (2017) 5282, https://doi.org/10.3748/wjg.v23.i29.5282.

[4] C. Verslype, E. van Cutsem, M. Dicato, N. Arber, J.D. Berlin, D. Cunningham, A. de Gramont, E. Diaz-Rubio, M. Ducreux, T. Gruenberger, D. Haller, K. Haustermans, P. Hoff, D. Kerr, R. Labianca, M. Moore, B. Nordlinger, A. Ohtsu, P. Rougier, W. Scheithauer, H.-J. Schmoll, A. Sobrero, J. Tabernero, C. van de Velde, The management of hepatocellular carcinoma. Current expert opinion and recommendations derived from the 10th World Congress on Gastrointestinal Cancer, Barcelona, 2008, Ann. Oncol. 20 (2009) vii1–vii6, https://doi.org/10.1093/annonc/mdp281.

[5] J.M. Llovet, M. Schwartz, V. Mazzaferro, Resection and liver transplantation for hepatocellular carcinoma, Semin. Liver Dis. 25 (2005) 181–200, https://doi.org/10.1055/s-2005-871198.

[6] J.M. Llovet, V. Hernandez-Gea, Hepatocellular carcinoma: reasons for phase III failure and novel perspectives on trial design, Clin. Cancer Res. 20 (2014) 2072–2079, https://doi.org/10.1158/1078-0432.CCR-13-0547.

[7] S. Zhang, W. Gao, J. Tang, H. Zhang, Y. Zhou, J. Liu, K. Chen, F. Liu, W. Li, S.K. Y. To, A.S.T. Wong, X. Zhang, H. Zhou, J.-Z. Zeng, The roles of GSK-3β in regulation of retinoid signaling and sorafenib treatment response in hepatocellular carcinoma, Theranostics 10 (2020) 1230–1244, https://doi.org/10.7150/thno.38711.

[8] J.M. Llovet, S. Ricci, V. Mazzaferro, P. Hilgard, E. Gane, J.-F. Blanc, A.C. de Oliveira, A. Santoro, J.-L. Raoul, A. Forner, M. Schwartz, C. Porta, S. Zeuzem, L. Bolondi, T.F. Greten, P.R. Galle, J.-F. Seitz, I. Borbath, D. Häussinger, T. Giannaris, M. Shan, M. Moscovici, D. Voliotis, J. Bruix, Sorafenib in advanced hepatocellular carcinoma, N. Engl. J. Med. 359 (2008) 378–390, https://doi.org/10.1056/NEJMoa0708857.

[9] J.A. Fagin, S.A. Wells, Biologic and clinical perspectives on thyroid cancer, N. Engl. J. Med. 375 (2016) 1054–1067, https://doi.org/10.1056/NEJMra1501993.

[10] H. Gleiter, Nanostructured materials: basic concepts and microstructure, Acta Mater. 48 (2000) 1–29, https://doi.org/10.1016/S1359-6454(99)00285-2.

[11] L.C. Costello, R.B. Franklin, Decreased zinc in the development and progression of malignancy: an important common relationship and potential for prevention and treatment of carcinomas, Expert Opin. Ther. Targets 21 (2017) 51–66, https://doi.org/10.1080/14728222.2017.1265506.

[12] M. Kumar, G.G. Meshram, T. Rastogi, S. Sharma, R. Gupta, S. Jain, A. Prasad, V. Galav, S.K. Bhattacharya, Antiangiogenic activity of zinc and zinc-sorafenib combination using the chick chorioallantoic membrane assay: a descriptive study, Int. J. Basic Clin. Pharmacol. 6 (2017) 1060, https://doi.org/10.18203/2319-2003.ijbcp20171559.

[13] H. Tian, M. Zhang, G. Jin, Y. Jiang, Y. Luan, Cu-MOF chemodynamic nanoplatform via modulating glutathione and H2O2 in tumor microenvironment for amplified cancer therapy, J. Colloid Interface Sci. 587 (2021) 358–366, https://doi.org/10.1016/j.jcis.2020.12.028.

[14] X. Sun, M. Keywanlu, R. Tayebee, Experimental and molecular dynamics simulation study on the delivery of some common drugs by ZIF-67, ZIF-90, and ZIF-8 zeolitic imidazolate frameworks, Appl. Organomet. Chem. 35 (2021), https://doi.org/10.1002/aoc.6377.

[15] Y. Pan, Y. Liu, G. Zeng, L. Zhao, Z. Lai, Rapid synthesis of zeolitic imidazolate framework-8 (ZIF-8) nanocrystals in an aqueous system, Chem. Commun. 47 (2011), https://doi.org/10.1039/c0cc05002d, 2071.

[16] H. Kaur, G.C. Mohanta, V. Gupta, D. Kukkar, S. Tyagi, Synthesis and characterization of ZIF-8 nanoparticles for controlled release of 6-mercaptopurine drug, J. Drug Deliv. Sci. Technol. 41 (2017) 106–112, https://doi.org/10.1016/j.jddst.2017.07.004.

[17] M. Hoop, C.F. Walde, R. Riccò, F. Mushtaq, A. Terzopoulou, X.-Z. Chen, A. J. deMello, C.J. Doonan, P. Falcaro, B.J. Nelson, J. Puigmartí-Luis, S. Pané, Biocompatibility characteristics of the metal organic framework ZIF-8 for therapeutical applications, Appl. Mater. Today 11 (2018) 13–21, https://doi.org/10.1016/j.apmt.2017.12.014.

[18] Y. Chu, J. Hou, C. Boyer, J.J. Richardson, K. Liang, J. Xu, Biomimetic synthesis of coordination network materials: recent advances in MOFs and MPNs, Appl. Mater. Today 10 (2018) 93–105, https://doi.org/10.1016/j.apmt.2017.12.009.

[19] R. Yogamalar, R. Srinivasan, A. Vinu, K. Ariga, A.C. Bose, X-ray peak broadening analysis in ZnO nanoparticles, Solid State Commun. 149 (2009) 1919–1923, https://doi.org/10.1016/j.ssc.2009.07.043.

[20] K.S. Park, Z. Ni, A.P. Côté, J.Y. Choi, R. Huang, F.J. Uribe-Romo, H.K. Chae, M. O'Keeffe, O.M. Yaghi, Exceptional chemical and thermal stability of zeolitic imidazolate frameworks, Proc. Natl. Acad. Sci. USA 103 (2006) 10186–10191, https://doi.org/10.1073/pnas.0602439103.

[21] J. Cravillon, S. Münzer, S.-J. Lohmeier, A. Feldhoff, K. Huber, M. Wiebcke, Rapid room-temperature synthesis and characterization of nanocrystals of a prototypical zeolitic imidazolate framework, Chem. Mater. 21 (2009) 1410–1412, https://doi.org/10.1021/cm900166h.

[22] X. Mi, M. Hu, M. Dong, Z. Yang, X. Zhan, X. Chang, J. Lu, X. Chen, Folic acid decorated zeolitic imidazolate framework (ZIF-8) loaded with baicalin as a nano-drug delivery system for breast cancer therapy, Int. J. Nanomed. 16 (2021) 8337–8352, https://doi.org/10.2147/IJN.S340764.

[23] K.S. Park, Z. Ni, A.P. Côté, J.Y. Choi, R. Huang, F.J. Uribe-Romo, H.K. Chae, M. O'Keeffe, O.M. Yaghi, Exceptional chemical and thermal stability of zeolitic imidazolate frameworks, Proc. Natl. Acad. Sci. USA 103 (2006) 10186–10191, https://doi.org/10.1073/pnas.0602439103.

[24] J. dos Santos Ferreira da Silva, D. López Malo, G. Anceski Bataglion, M. Nogueira Eberlin, C. Machado Ronconi, S. Alves Júnior, G.F. de Sá, Adsorption in a fixed-bed column and stability of the antibiotic oxytetracycline supported on Zn(II)-[2-Methylimidazolate] frameworks in aqueous media, PLoS One 10 (2015), e0128436, https://doi.org/10.1371/journal.pone.0128436.

[25] Z. Ferdous, A. Nemmar, Health impact of silver nanoparticles: a review of the biodistribution and toxicity following various routes of exposure, Int. J. Mol. Sci. 21 (2020), https://doi.org/10.3390/ijms21072375.

[26] J. Ran, C. Wang, J. Zhang, W. Wang, L. Xiao, S. Jia, Z. Wang, W. Wu, J. Xiao, X. Wu, New insight into Polydopamine@ZIF-8 nanohybrids: a zinc-releasing container for potential anticancer activity, Polymers 10 (2018), https://doi.org/10.3390/polym10050476.

[27] C. Schult, M. Dahlhaus, S. Ruck, M. Sawitzky, F. Amoroso, S. Lange, D. Etro, A. Glass, G. Fuellen, S. Boldt, O. Wolkenhauer, L.M. Neri, M. Freund, C. Junghanss, The multikinase inhibitor Sorafenib displays significant antiproliferative effects and induces apoptosis via caspase 3, 7 and PARP in B- and T-lymphoblastic cells, BMC Cancer 10 (2010) 560, https://doi.org/10.1186/1471-2407-10-560.

[28] M. Tomizawa, F. Shinozaki, T. Sugiyama, S. Yamamoto, M. Sueishi, T. Yoshida, Sorafenib suppresses the cell cycle and induces the apoptosis of hepatocellular carcinoma cell lines in serum-free media, Exp. Ther. Med. 1 (2010) 863–866, https://doi.org/10.3892/etm.2010.131.

[29] M.A. Park, G. Zhang, A.P. Martin, H. Hamed, C. Mitchell, P.B. Hylemon, M. Graf, M. Rahmani, K. Ryan, X. Liu, S. Spiegel, J. Norris, P.B. Fisher, S. Grant, P. Dent, Vorinostat and sorafenib increase ER stress, autophagy and apoptosis via ceramide-dependent CD95 and PERK activation, Cancer Biol. Ther. 7 (2008) 1648–1662, https://doi.org/10.4161/cbt.7.10.6623.